



Infiltrating Mast Cell–Mediated Stimulation of Estrogen Receptor Activity in Breast Cancer Cells Promotes the Luminal Phenotype

Maria Teresa Majorini¹, Valeria Cancila², Alice Rigoni¹, Laura Botti¹, Matteo Dugo³, Tiziana Triulzi⁴, Loris De Cecco³, Enrico Fontanella¹, Elena Jachetti¹, Elda Tagliabue⁴, Claudia Chiodoni¹, Claudio Tripodo², Mario P. Colombo¹, and Daniele Lecis¹

ABSTRACT

Tumor growth and development is determined by both cancer cell–autonomous and microenvironmental mechanisms, including the contribution of infiltrating immune cells. Because the role of mast cells (MC) in this process is poorly characterized and even controversial, we investigated their part in breast cancer. Crossing C57BL/6 MMTV–PyMT mice, which spontaneously develop mammary carcinomas, with MC-deficient C57BL/6–Kit^{W-sh/W-sh} (Wsh) mice, showed that MCs promote tumor growth and prevent the development of basal CK5-positive areas in favor of a luminal gene program. When cocultured with breast cancer cells *in vitro*, MCs hindered activation of cMET, a master regulator of the basal program, and simultaneously promoted expression and activation of estrogen receptor (*ESR1/ER*) and its target genes (*PGR*, *KRT8/CK8*, *BCL2*), which are all luminal markers. Moreover, MCs reduced

ERBB2/HER2 levels, whose inhibition further increased *ESR1* expression. *In vivo* and *in silico* analysis of patients with breast cancer revealed a direct correlation between MC density and *ESR1* expression. In mice engrafted with HER2-positive breast cancer tumors, coinjection of MCs increased tumor engraftment and outgrowth, supporting the link between MCs and increased risk of relapse in patients with breast cancer. Together, our findings support the notion that MCs influence the phenotype of breast cancer cells by stimulating a luminal phenotype and ultimately modifying the outcome of the disease.

Significance: Mast cells impact breast cancer outcome by directly affecting the phenotype of tumor cells through stimulation of the estrogen receptor pathway.

Introduction

Breast cancer is the most frequent type of tumor (1) and is responsible for more than 600,000 deaths/year worldwide. Breast cancer is an extremely heterogeneous disease, which can be molecularly classified on the basis of gene expression in different subgroups endowed with predictive and prognostic value. The most widely employed signature, referred to as PAM50, clusters breast cancers in five subgroups: luminal A, luminal B, HER2-enriched, basal-like, and normal (2). Nonetheless, in the clinical practice, breast cancer subtypes are usually defined by evaluating the expression of marker proteins, being hormone receptors (HR) and *ERBB2/HER2* the most exploited. Tumors that express HR [estrogen (ER) and/or progesterone (PR)

receptors] mainly belong to the luminal subtypes (A or B), while tumors that do not express ER and PR are classified as HER2-positive or triple-negative according to the overexpression or lack of HER2, respectively (3). Even though the molecular-intrinsic and IHC-based classifications do not entirely match (3), the expression of HR and HER2 has profound implications in terms of tumor biology, clinical outcome, and choice of therapy (4).

Along with cell-autonomous features, cancer aggressiveness and outcome are also determined by the intricate cross-talk of cancer cells with the surrounding microenvironment made of extracellular matrix (ECM), soluble factors, and infiltrating cells. In particular, there is growing interest towards the interaction between cancer and immune cells because tumors develop a plethora of mechanisms to escape from immune system surveillance (5), or even hijack it, to grow and disseminate. Accordingly, the analysis of the immune tumor infiltration displays predictive and prognostic value (6–8), also in patients with breast cancer (9–11). The presence of various immune subpopulations or specific phenotypes, such as myeloid-derived suppressor cells (MDSC; ref. 12) or M2-polarized macrophages (13, 14), have been clearly associated with a protumor effect, whereas T lymphocytes with a more favorable prognosis (15, 16). Other immune cell populations are less studied and their role remains uncertain because of controversial results, as in the case of mast cells (MC). In fact, the impact of MCs could change among the different breast cancer subtypes (17) and vary according to tumor grade. It has also been proposed that MCs could display a protective effect before tumor onset, but sustain its development at later stages (18).

MCs are bone marrow–derived c-Kit expressing immune cells classically known for their role in allergic reactions (19). MCs usually localize at boundaries of the body, such as mucosa and skin, and can be found in proximity of blood vessels, nerve endings, and stromal tissue. Here, they occupy a privileged position as sensors of tissue

¹Molecular Immunology Unit, Department of Research, Fondazione IRCCS Istituto Nazionale dei Tumori, Milan, Italy. ²Tumor Immunology Unit, Department of Health Sciences, Human Pathology Section, University of Palermo School of Medicine, Palermo, Italy. ³Platform of Integrated Biology, Department of Applied Research and Technology Development, Fondazione IRCCS Istituto Nazionale dei Tumori, Milan, Italy. ⁴Molecular Targeting Unit, Department of Research, Fondazione IRCCS Istituto Nazionale dei Tumori, Milan, Italy.

Note: Supplementary data for this article are available at Cancer Research Online (<http://cancerres.aacrjournals.org/>).

#M.P. Colombo and D. Lecis contributed equally as co-last authors of this article.

Corresponding Authors: Daniele Lecis, Fondazione IRCCS Istituto Nazionale dei Tumori, Via Amadeo 42, Milan 20133, Italy. Phone: 3902-2390-2212; Fax: 3902-2390-2630; E-mail: daniele.lecis@istitutotumori.mi.it; and Mario P. Colombo, mariopao.colombo@istitutotumori.mi.it

Cancer Res 2020;80:2311–24

doi: 10.1158/0008-5472.CAN-19-3596

©2020 American Association for Cancer Research.

modifications and can trigger rapid and potent responses through their distinctive granules. MCs have recently been shown to affect cancer cells by direct interaction or through the modulation of ECM (20) and immune infiltrate (21, 22) in different tumor types. They have also been shown to influence breast cancer outcome and treatment efficacy (23), but the underlying mechanisms are still poorly characterized. With our work, we provide evidence that MCs can directly affect the features of adjacent breast cancer cells and drive basal cells toward a more luminal phenotype characterized by increased expression of ER, PGR, BCL2, and CK8. Simultaneously, MCs reduce the activation of HER2 and of basal drivers such as EGFR and cMET, and prevent the expression of the basal marker CK5, thus potentially affecting the behavior of neighboring cancer cells.

Materials and Methods

Cell cultures and reagents

Human MDA-MB231, BT549, and SKBr3 (all from ATCC) cell lines were cultured in RPMI1640 medium (Lonza Group) supplemented with 10% FBS (EuroClone), 2 mmol/L L-glutamine, sodium pyruvate (NaPyr), and nonessential amino acids (NEAA, all from Lonza). Human BT474 (ATCC) and mouse PyMT41c and N2C (24) cell lines were maintained in DMEM (Gibco-Thermo Fisher Scientific) supplemented with 10% FBS, 2 mmol/L L-glutamine, NaPyr, and NEAA. The HMC1.2 cell line was kindly provided by Carlo E. Pucillo (University of Udine, Udine, Italy) and was cultured in RPMI1640 medium supplemented with 10% FBS, L-glutamine, Hepes (Lonza), NaPyr, NEAA, and 2-mercaptoethanol (2ME). All cell lines were cultured at 37°C in fully humidified atmosphere with 5% CO₂ and monthly checked for *Mycoplasma* with a Mycoplasma Detection Kit (Takara). MDA-MB-231, BT-549, BT-474, and SKBr3 cell line authentication was performed before starting the experiments and confirmed on January 16, 2020 by Eurofins Genomics. The PyMT41c, WPY25F, and N2C were established in our laboratory from spontaneous tumors collected from PyMT B6, PyMT Wsh, and BALB/c Neu transgenic mice, respectively, as described previously (24). Briefly, spontaneous tumors were resected and minced with scissors after removing of fat, large vessels, and necrotic areas. Tumor tissues were digested in warm trypsin (37°C for 30 minutes) and then plated in DMEM with 20% FCS (Bio Whittaker) upon mechanical dissection through cell strainers. When established, cell lines were cultured in DMEM 10% FCS. A characterization of the cell lines is shown in Supplementary Fig. S1A.

Cell treatment and transfection

To stimulate a basal phenotype, cells were serum-starved overnight with medium supplemented with 0.1% FBS and then treated with 20 ng/mL EGF (catalog no. GRF-10544, Selleck Chemicals) or TGFβ (catalog no. 100-B, R&D Systems). Lipofectamine RNAiMAX (Thermo Fisher Scientific) reagent was used for siRNA transfections by employing a reverse transfection protocol described previously (25). The negative control siRNA Duplex (siCtr, #1027310) and FlexiTube siRNAs specific for cMET (#SI00300860 and #SI00300867) and HER2 (#SI00063882) were purchased from Qiagen.

Western blot analysis and phospho-RTK protein array

For Western blot analysis, cells were harvested, washed twice with ice-cold PBS, boiled for 10 minutes in lysis buffer (125 mmol/L Tris HCl, pH 6.8, 5% SDS), and then supplemented with protease inhibitors. Samples were sonicated, clarified at room temperature by centrifugation for 15 minutes at 11,000 rpm, and then quantified with BCA (Thermo Fisher Scientific). Cleared supernatants were separated

by SDS-PAGE on precast 4%–12% Bis-Tris NuPAGE gels (Thermo Fisher Scientific) and proteins transferred to polyvinylidene difluoride membranes (Merck Millipore) by using the XCell II blot module (Thermo Fisher Scientific). Membranes were then saturated for 30 minutes in Tris-buffered saline containing 4% BSA and incubated overnight with anti-human primary antibodies recognizing CK5 #ab53121, CK8 #ab59400, ERα #ab16460 (1:1,000, Abcam); phospho-cMET #44888g (1:1,000, Thermo Fisher Scientific); cMET (c-12) #sc-10, ERα (G-20) #sc-544 (1:500, Santa Cruz Biotechnology); human phospho-EGFR #2236, mouse phospho-EGFR #3777, phospho-ER (S167) #64508 (1:1,000, Cell Signaling Technology); GAPDH #WH0002597M1, actin #A1978, and vinculin #V9131 (1:5,000, Sigma-Aldrich). Antibody specific for BCL2 has been described previously (25). After incubation with the appropriate secondary antibody (anti-rabbit and anti-mouse IgG purchased from GE Healthcare, UK, and anti-goat IgG from Thermo Fisher Scientific; all secondary antibodies were diluted 1:2,000), proteins were detected by chemiluminescence (EuroClone).

Mouse phospho-RTK array (#ARY014) was purchased by R&D Systems. Membranes of the array were hybridized by using 300 µg of total protein extracts according to the manufacturer's guidelines.

Flow cytometry analysis

The phenotype of solid tumor and cultured cells was measured by flow cytometry analysis after washing with a buffer containing 2% BSA and staining with antimouse mAbs. The following antibodies were used: antiCD117/cKit (#11-1171-85), antiCD11b (#17-0112-83), antiCD49f (#12-0495-82; all from eBioscience), antiFcεRI (#60-1172-U100, Tonbo Biosciences), and anti-EpCAM (#563478; BD Biosciences). Samples were analyzed by using FACSCalibur (BD Biosciences) and LSRII Fortessa (BD Biosciences) instruments and analyzed with FlowJo software.

RNA extraction and real-time PCR

To perform real-time PCR, total RNA was extracted from cells with the miRNeasy Mini Columns (Qiagen) and 1 µg RNA was reverse-transcribed by using the High Capacity cDNA Reverse Transcription Kit (#4368814, Thermo Fisher Scientific). Probes for human *KRT8* (Hs_01595539_g1), *ESR1* (Hs_01046816_m1), *PGR* (Hs_01556702_m1), *GAPDH* (Hs_02786624_g1); mouse *Cpa3* (Mm00483940_m1), *ErbB2* (Rn01461185_m1), *Ms4a2* (Mm00442778_m1) and *Gapdh* (Mm99999915_g1) were purchased from Thermo Fisher Scientific. Probes for human *BCL2* (Hs_PT.56a.2905156) and for mouse *Krt5* (Mm_PT.58.41573083), *Esr1* (Mm_PT.58.8025728), *Pgr* (Mm_PT.58.10254276) were purchased from IDT. Real-time PCR was carried out with TaqMan Fast universal PCR Master Mix (#4352042, Thermo Fisher Scientific) and samples were analyzed by QuantStudio 3 (Thermo Fisher Scientific). All transcript levels were quantified by using the ΔC_t method and normalized to GAPDH expression.

Immunofluorescence

For immunofluorescence analysis, cells were fixed for 10 minutes with 4% paraformaldehyde, permeabilized for 10 minutes at room temperature with 0.2% Triton X-100 and blocked in PBS, 3% BSA, and 0.1% Tween-20. Coverslips were then incubated overnight at 4°C in a humidified chamber with antibodies directed to ER (Santa Cruz Biotechnology # sc-544, rabbit, dilution 1:200) and nuclei colored with DAPI. Fluorescent images were acquired with a Leica DM4 B optical microscope equipped with a DFC450 digital camera.

Bone marrow-derived MC differentiation and characterization

Bone marrow (BM) cells were harvested from the femurs of C57BL/6 or BALB/c mice. Femurs were dissected to remove any muscle fragment and one extremity was cut with sterile scissors. BM cells were flushed out by using the needle of a 10 mL syringe, previously filled with sterile PBS, and inserted in the medullar canal. The cell suspension was cultured *in vitro* in RPMI with 20% FBS, supplemented with 20 ng/mL SCF and IL3 (PeproTech). Once a week, nonadherent cells were centrifuged, resuspended in fresh culture medium, and placed in new culture flasks. After 3 weeks, BMMC purity was evaluated by flow cytometry (FACS) by measuring the percentage of FcεRIβ and cKitpositive cells. BMNCs were employed for *in vitro* or *in vivo* experiments only if culture purity was >90% (Supplementary Fig. S1B). Degranulation was evaluated by staining with anti CD107a antibody (#20-1071-82, eBioscience). As a positive control, BMNCs were stimulated with 500 ng/mL ionomycin (catalog no. I0634, Sigma-Aldrich) for 30 minutes. The activation of ER of breast cancer cell cocultured with BMNCs was inhibited by treatment with 10 μmol/L 4-hydroxytamoxifen (4-OHT, # H6278, Sigma-Aldrich) for 4 hours.

Mice and treatments

C57BL/6 MMTV-PyMT (PyMT B6) mice (26) were purchased from The Jackson Laboratory and backcrossed with C57BL/6-Kit^{W-sh/W-sh} (Wsh; The Jackson Laboratory) mice, which lack MCs due to a genetic inversion within the cKit promoter gene (27) in the “white spotting locus”, and are hence characterized by a white coat. Mice were maintained under pathogenfree conditions at the animal facility of Fondazione IRCCS Istituto Nazionale dei Tumori (Milan, Italy). Experiments were approved by the Ethics Committee for Animal Experimentation of the Fondazione IRCCS Istituto Nazionale dei Tumori of Milan according to institutional guidelines and to the Italian Law (D.lgs 26/2014). *In vivo* experiments were approved by the Italian Ministry of Health (authorization numbers 1028/2016-PR, 474/2017-PR and 218/2018-PR). Tumors were measured by caliper and volume calculated with the formula $V = d \times d \times D/2$ where “d” represents the minor and “D” the major diameter.

In coinjection *in vivo* experiments, BALB/c mice were engrafted with 1.8×10^5 N2C cells alone or coinjected with MCs previously prepared from the BM of the same mouse strain. Recombinant mouse anti-rat HER2 antibody (7.16.4) was purchased from BioCell (catalog no. BE027) and administered intraperitoneally (i.p., 5 mg/kg in saline) at days 7, 11, 14, and 19. Mice were sacrificed 26 days after the engraftment.

Histology and IHC

Tumors samples were fixed in formalin and embedded in paraffin. Four-micron-thick sections were cut and used for both histopathology (hematoxylin & eosin) and immunostainings. IHC was performed by using a horseradish peroxidase methods. The antigen unmasking technique was performed by using Novocastra Epitope Retrieval Solutions pH6 in PT Link Dako at 98°C for 30 minutes. Subsequently, the sections were brought to room temperature and washed in PBS. After neutralization of the endogenous peroxidase with 3% H₂O₂ and Fc blocking by a specific protein block, the samples were incubated overnight at 4°C with the following primary antibodies: Rabbit monoclonal CK5 (clone EP1601Y; 1:100 pH6; Abcam). Staining was revealed by using IgG (H&L) specific secondary antibodies (Life Technologies, 1:500) and AEC (3-Amino-9-Ethylcarbazole) was used as substrate chromogen. The slides were counterstained with Harris hematoxylin (Novocastra). All sections were analyzed under a Zeiss

AXIO Scope.A1 microscope (Zeiss) and microphotographs were collected by using a Zeiss Axiocam 503 Color digital camera using the Zen2 imaging software. The grade of mouse mammary carcinomas was assessed by evaluating the degree of nuclear atypia and glandular formation pattern. MC presence in mouse mammary gland tumor was detected through toluidine blue staining (28).

Gene expression profiling and bioinformatics

Total RNA was extracted with the RNeasy Lipid Tissue Mini Kit (Qiagen) according to the manufacturer's instructions. RNA quality was assessed by using TapeStation (Agilent) and was quantified with Qubit (Thermo Fisher Scientific). Total RNA was amplified by employing the Agilent Low Input Quick Amp WT labeling kit according to the manufacturer's instructions. Briefly, 100 ng of total RNA was used to synthesize doublestranded cDNA, which was translated into cRNA in the presence of Cy3-dCTP and amplified by T7 RNA polymerase. Fluorescent dye-labeled cRNA was hybridized to Agilent SurePrint G3 Mouse GE v2 8 × 60K microarrays. Hybridization and washing were performed according to Agilent standard protocols. Microarray images were acquired with the Agilent DNA microarray scanner. Raw gene expression data were generated by Agilent Feature Extraction software v10.7.3.1 and were preprocessed with the limma package (29). Briefly, raw data were log₂-transformed, background-corrected through the normexp method and quantile-normalized. Probes detected in less than three samples, according to the *IsPosAndSignif* flag, were filtered out. Replicated probes were summarized by calculating their average expression. Probes representing the same gene were collapsed by selecting the probe with highest variance across samples. Gene expression data were deposited in the NCBI Gene Expression Omnibus (GEO) with accession number GSE139568.

Differentially expressed genes were identified by using *limma* (29). *P* values were corrected for multiple testing with the Benjamini-Hochberg false discovery rate (FDR) method. Genes with an FDR < 0.05 were selected.

Gene expression and clinical data of METABRIC (30) were downloaded from the cBioPortal website (<http://www.cbioportal.org/>) with accession date February 28, 2019. For the GHEA cohort (31), processed data for 36 patients who did not receive neoadjuvant therapy were downloaded from GEO with accession number GSE55348. The abundance of tumor-infiltrating MCs was calculated as the sum of “Mast Cells Resting” and “Mast Cells Activated” cell fractions estimated by CIBERSORT (32) in absolute mode. For METABRIC, only samples with a CIBERSORT *P* < 0.05 were considered for downstream analyses.

Gene set enrichment analysis (GSEA; ref. 33) was performed in preranked mode by employing the fgsea Bioconductor package with Hallmark gene sets or gene sets related to basal or luminal breast cancer selected from the C2-CPG collection of the MSigDb database (<http://software.broadinstitute.org/gsea/msigdb/index.jsp>). Genes from the microarray mouse data were preranked according to the limma *t*-statistic calculated between PyMT B6 and PyMT Wsh mice. Genes of METABRIC were preranked according to the Spearman correlation coefficient with CIBERSORT MC estimates. Gene sets with an FDR < 0.05 were selected.

Graphs and statistical analysis

Graphs and statistical analysis was performed using GraphPad Prism 8.2.0. Association between continuous and categorical variables was evaluated by two-tailed paired and unpaired Student *t* test or one-way ANOVA. For noncontinuous variables, the two-tailed Mann-

Whitney test was employed. Association between continuous variables was assessed by using Spearman correlation coefficient.

Results

MCs increase breast cancer growth and metastasis

To investigate the effect of MCs in affecting breast cancer growth and phenotype, we crossed C57BL/6 MMTV-PyMT (PyMT B6) mice with C57BL/6-Kit^{W-sh/W-sh} (Wsh) mice, which lack MCs (Fig. 1A) due to an inversion of the c-Kit promoter (27). As expected, only mammary tumors developed in PyMT B6 mice were positive for MC staining, while PyMT Wsh nodules lacked MCs. MCs localized especially in the stromal region surrounding mammary tumor nodules in close contact with the basal layer while a few MCs infiltrated the tumor tissue (Fig. 1A). PyMT Wsh mice developed delayed palpable tumors compared with mice with MCs (Fig. 1B) and, consequently, showed tumors significantly smaller (Fig. 1C). Tumor analyses confirmed that the absence of MCs caused the development of mammary tumors characterized by a lower grade (Fig. 1D). Because MMTV-PyMT mice develop spontaneous metastases, we also analyzed lungs from PyMT B6 and PyMT Wsh mice and, in line with what was observed with primary tumor growth and grade, we observed that the lack of MCs reduced metastasis dissemination (Fig. 1E–H). Given that primary tumors were not surgically removed, the augmented number of metastasis is more likely ascribable to the earlier onset of primary tumors in PyMT B6 mice and to their enlargement, and not to enhanced intrinsic metastasizing features of cancer cells. In conclusion, in the PyMT model, the presence of MCs favors the onset of spontaneous mammary tumors, which hence grow faster, reach a higher grade, and form metastasis earlier than MC-lacking Wsh mice.

The absence of MCs favors the development of tumors with a basal phenotype

We then tested whether tumors arising in the two different microenvironments, characterized by the presence or the absence of MCs, showed phenotypical differences beyond tumor grade. Histopathologic analysis on hematoxylin and eosin-stained sections revealed that a fraction of PyMT Wsh showing high histologic grade characterized by nests and trabeculae of malignant cells with high cytologic atypia had signs of squamous metaplasia (Fig. 2A). This peculiar morphology was consistently associated with the increase of areas characterized by a basal phenotype according to CK5 immunostaining (Fig. 2B). Indeed, the basal layer of neoplastic glands in Wsh tumors foci was maintained along tumor progression with overtly infiltrating tumors displaying an increase in areas of CK5-expressing cells as compared with their wild-type counterparts, where basal areas were only focally represented (Fig. 2B and C). To further test the capability of MCs to affect the phenotype of breast cancer cells, we also employed an independent transplantable tumor approach by injecting the PyMT Wsh-derived WPY25F cell line in the fat pad of either C57BL/6 MC-proficient (B6) or -deficient (Wsh) mice. Phenotype characterization was carried out by flow cytometry analysis of single-cell suspensions obtained from *ex vivo* nodules, which were stained with EpCAM and CD49f. The FACS analysis confirmed the increase of basal cells, which can be identified as CD49f^{high} EpCAM^{low}, in cancer cells grown in MC-deficient Wsh mice (Fig. 2D, gating strategy in Supplementary Fig. S1C). Therefore, on the one hand, the presence of MCs promotes the growth of primary tumors, and on the other, their absence favors the development and/or the maintenance of basal areas.

MCs correlate with lower CK5 levels and reduce its expression *in vitro*

Having shown that MCs are inversely linked to a basal phenotype, we investigated whether this correlation exists also in human tumors. *In silico* analysis of METABRIC gene expression data confirmed that MCs are more infiltrated in luminal hormone receptor-positive breast cancer (i.d. luminal A and B, Fig. 3A), which express higher levels of the luminal marker KRT8/CK8, while the basal marker KRT5/CK5 is downregulated in luminal (ER positive) and HER2-positive breast cancers (Fig. 3B). We then tested the capacity of MCs to affect the expression of CK5 and CK8 *in vitro* in coculture experiments finding that MCs reduced the levels of CK5 both at transcription (Fig. 3C) and protein (Fig. 3D) levels. Simultaneously, the expression levels of CK8 were increased by MC coculturing (Fig. 3C). These observations were made both in human breast cancer (BT474 and SKBr3 considered models of HR⁺/HER2⁺ and HR⁻/HER2⁺ breast cancer, respectively) and in mouse tumor-derived cell lines (N2C and PyMT41c). To further test the capacity of MCs to prevent the expression of CK5 and, simultaneously, trigger CK8, we stimulated MDA-MB-231 (human triple-negative), BT474, and PyMT41c breast cancer cell lines with TGFβ, which promotes CK5 and inhibits CK8 expression (Fig. 3E and F). In agreement with our previous findings, MCs coculturing prevented the effect of TGFβ on the expression of CK5 and, simultaneously, triggered CK8 expression. Therefore, MCs stimulate a luminal phenotype, highlighted by CK8 expression, and simultaneously prevent the expression of the basal CK5 marker in breast cancer cell lines.

MCs reduce the activation of cMET and EGFR receptors

cMET, together with EGFR, is a master regulator of the basal program and, accordingly, it is highly expressed in triple-negative breast cancers, which are often characterized by a basal-like phenotype (Fig. 4A). Because MC peptidases have been shown to cleave cMET ligand HGF into an NK4-like inhibitory molecule (34), we tested whether the presence of MCs could affect the activation of cMET. In agreement with our hypothesis, the phosphorylation of cMET, and not its expression level, was reduced by MCs in a panel of human breast cancer cell lines cocultured with both BMMCs (Fig. 4B, left and middle) or a human MC cell line (HMC1.2, Fig. 4B, right). Notably, also the activation of EGFR, another basal marker, was inhibited by MC presence (Fig. 4C). Of note, the role of cMET and EGFR in promoting the basal, while inhibiting the luminal, phenotype was confirmed by silencing experiments. In fact, while stimulation with EGF promoted CK5 expression, the depletion of cMET reduced its expression (Fig. 4D, top). At the same time, MCs could stimulate CK8 expression and this effect was further amplified by concomitant cMET silencing (Fig. 4D, bottom). Therefore, the capability of MCs to hinder the basal program could be also due to their inhibitory effect of cMET activation. Because the activation of MCs can eventually result in their degranulation, we asked whether this process was necessary to stimulate the observed phenotypes, that is, increase of CK8 levels, inhibition of CK5 expression, and EGFR/cMet activation. Therefore, MCs used in the coculture experiments as described above were collected and analyzed by flow cytometry to quantify the percentage of degranulated MCs. By measuring the levels of exposed CD107a, we concluded that the presence of cancer cells did not stimulate the degranulation of MCs, which was less than 1% and comparable with unstimulated BMMCs. Nevertheless, BMMCs were indeed proficient to degranulate, as assessed through

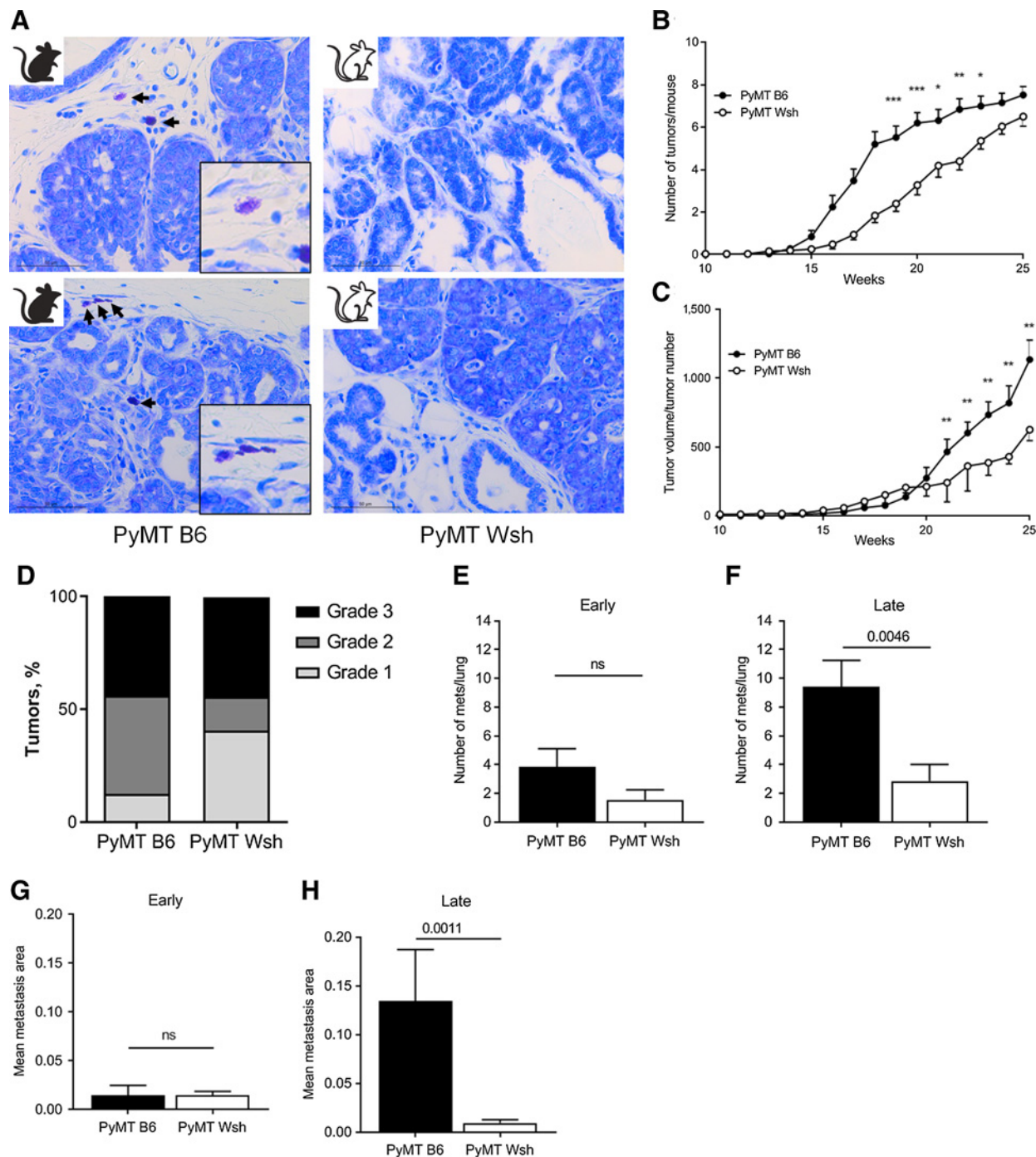


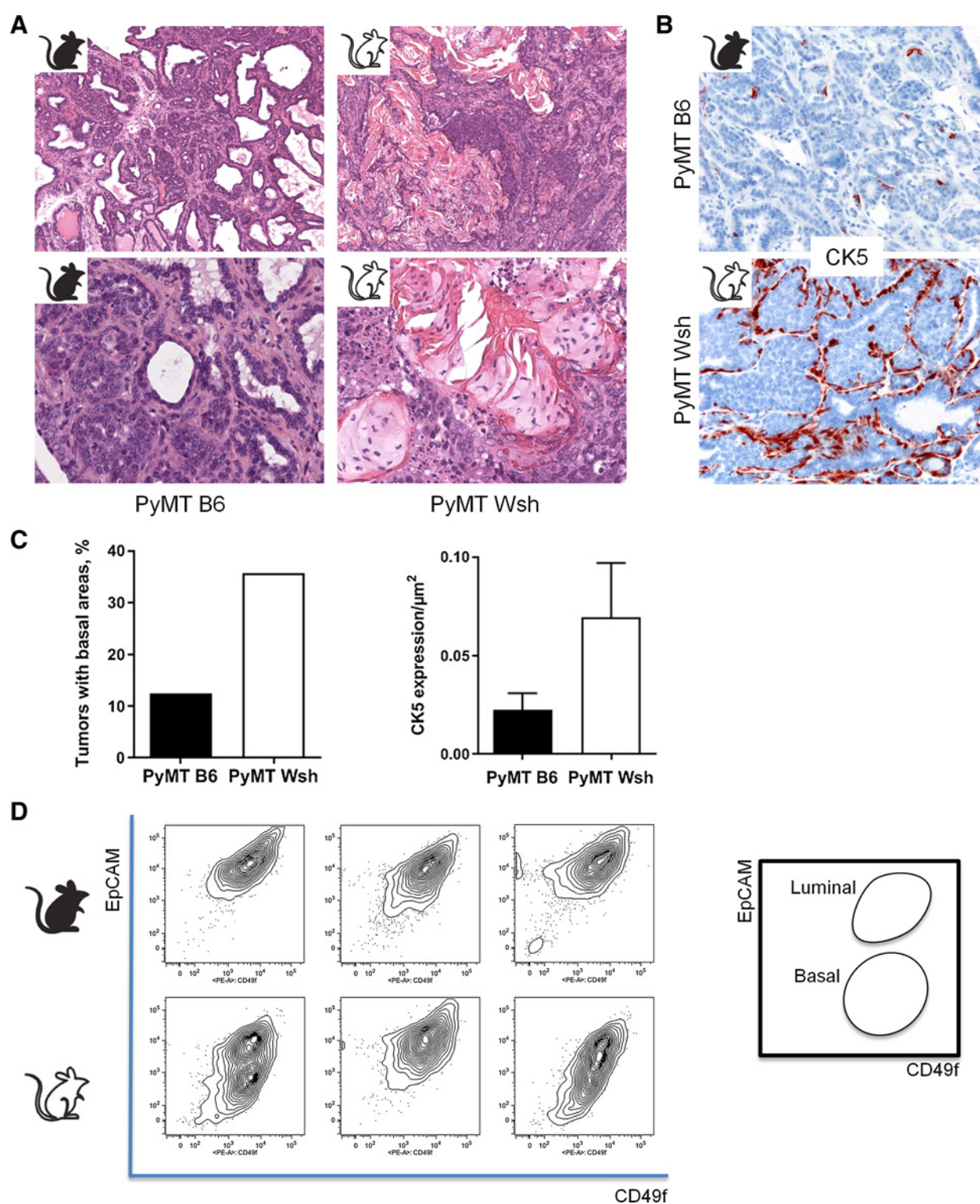
Figure 1.

MCs promote growth of spontaneous primary mammary tumors. **A**, Blue toluidine staining of mammary tumors collected from two MC-proficient (B6, black coat, left) and two MC-deficient (Wsh, white coat, right) MMTV-PyMT transgenic mice. **B** and **C**, Spontaneous mammary tumors were counted (**B**) and volumes measured (**C**) in either B6 or Wsh PyMT mice. **D**, At the end of the experiments, mice were euthanized and primary tumors collected for IHC evaluation. **E-H**, In addition, lungs were collected and hematoxylin and eosin stained to evaluate the number (**E** and **F**) and the size (**G** and **H**) of spontaneous metastasis both at early (mice of 18–20 weeks) and late (24–25 weeks) stages of tumor development. ns, nonsignificant.

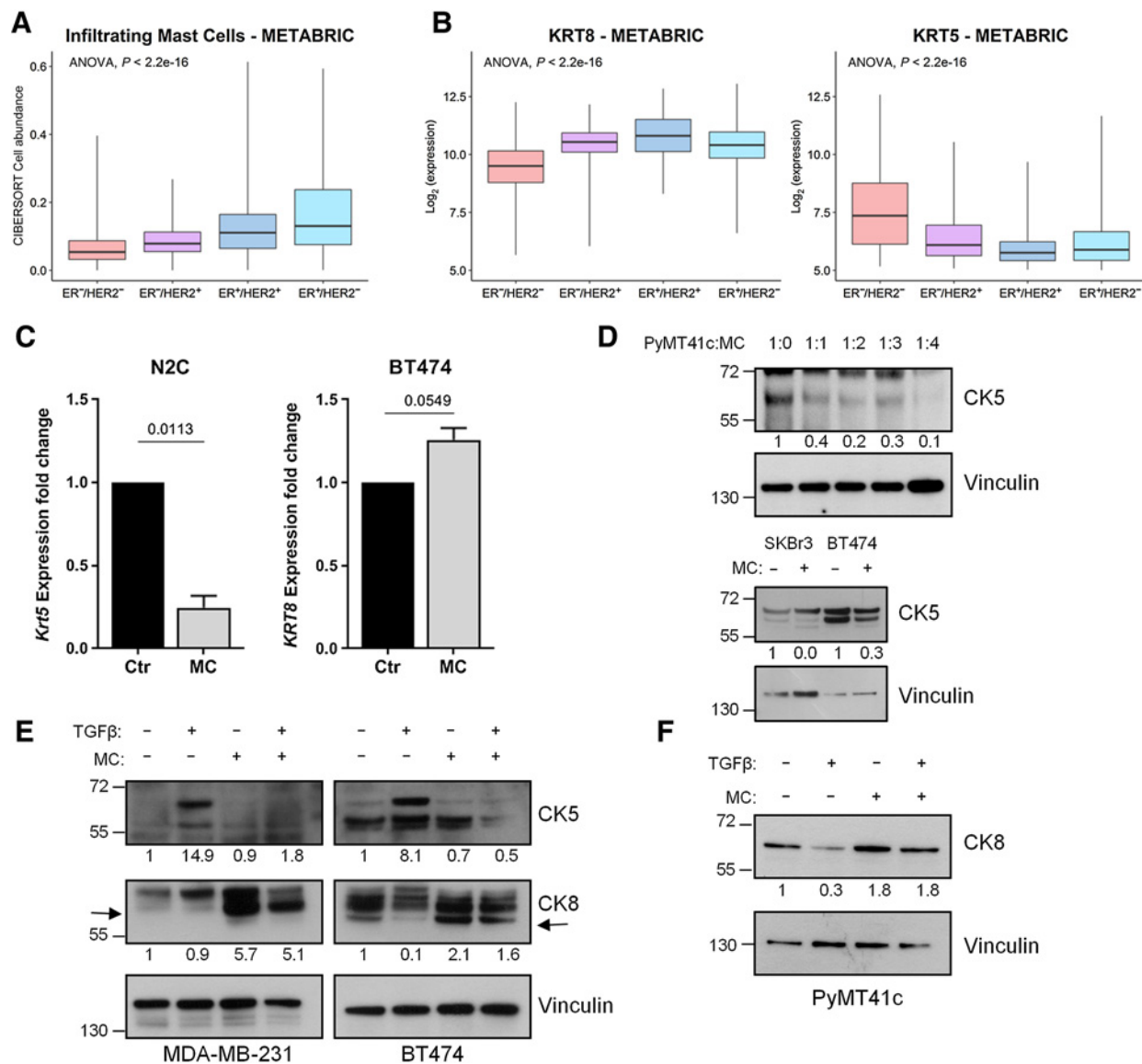
in vitro stimulation with ionomycin (Fig. 4E). Hence, our data strongly support the notion that the observed phenotypic changes of cancer cells cocultured with MCs are independent of the release of MC granules.

MCs stimulate the expression and activity of ER

Luminal breast cancer cells can be identified by CK expression and are characterized by the expression of HR, in particular estrogen receptor (ER). This receptor is exploited in the clinics for breast cancer

**Figure 2.**

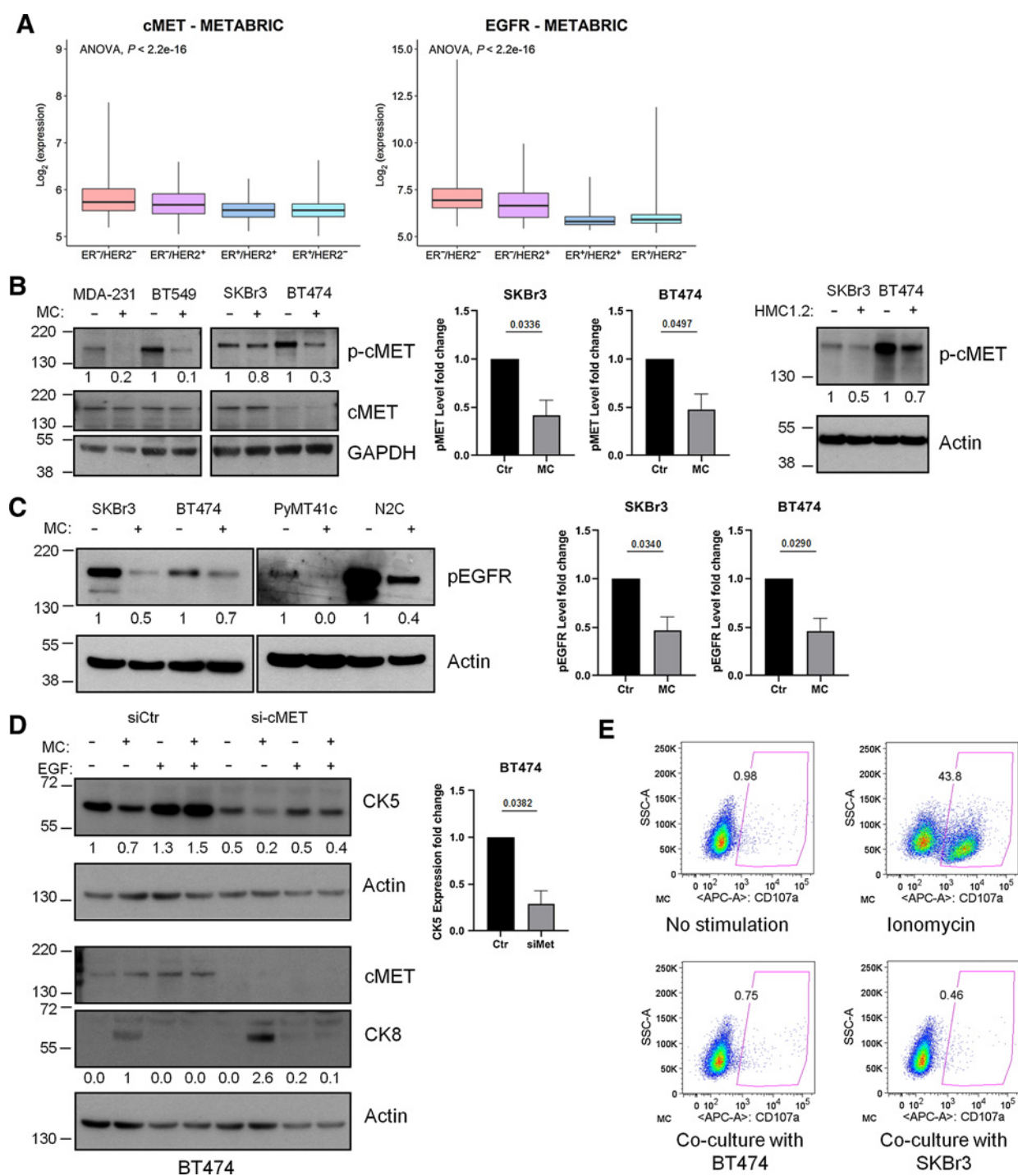
The absence of MCs favors squamous metaplasia and the expression of basal linings/areas in tumor nests and trabeculae of Wsh mice. **A**, Representative microphotographs of hematoxylin and eosin histologies from high-grade PyMT B6 (left) and PyMT Wsh (right) tumors showing the presence of foci of squamous metaplasia in the Wsh setting (×10, top; ×40, bottom). **B**, CK5 staining of PyMT B6 (top) and PyMT Wsh (bottom) high-grade tumors highlighting the increased density and diffuse distribution of CK5⁺ areas in Wsh tumors. **C**, Percentage of tumors that develop CK5-positive regions in PyMT B6 and PyMT Wsh mice (left) and measurement of their size (right). **D**, The PyMT Wsh tumor-derived cell line WPY25F was injected subcutaneously in B6 and Wsh mice and left to grow. Tumors were then collected and analyzed by FACS to evaluate the luminal and basal phenotype with EpCAM/CD49f staining.

**Figure 3.**

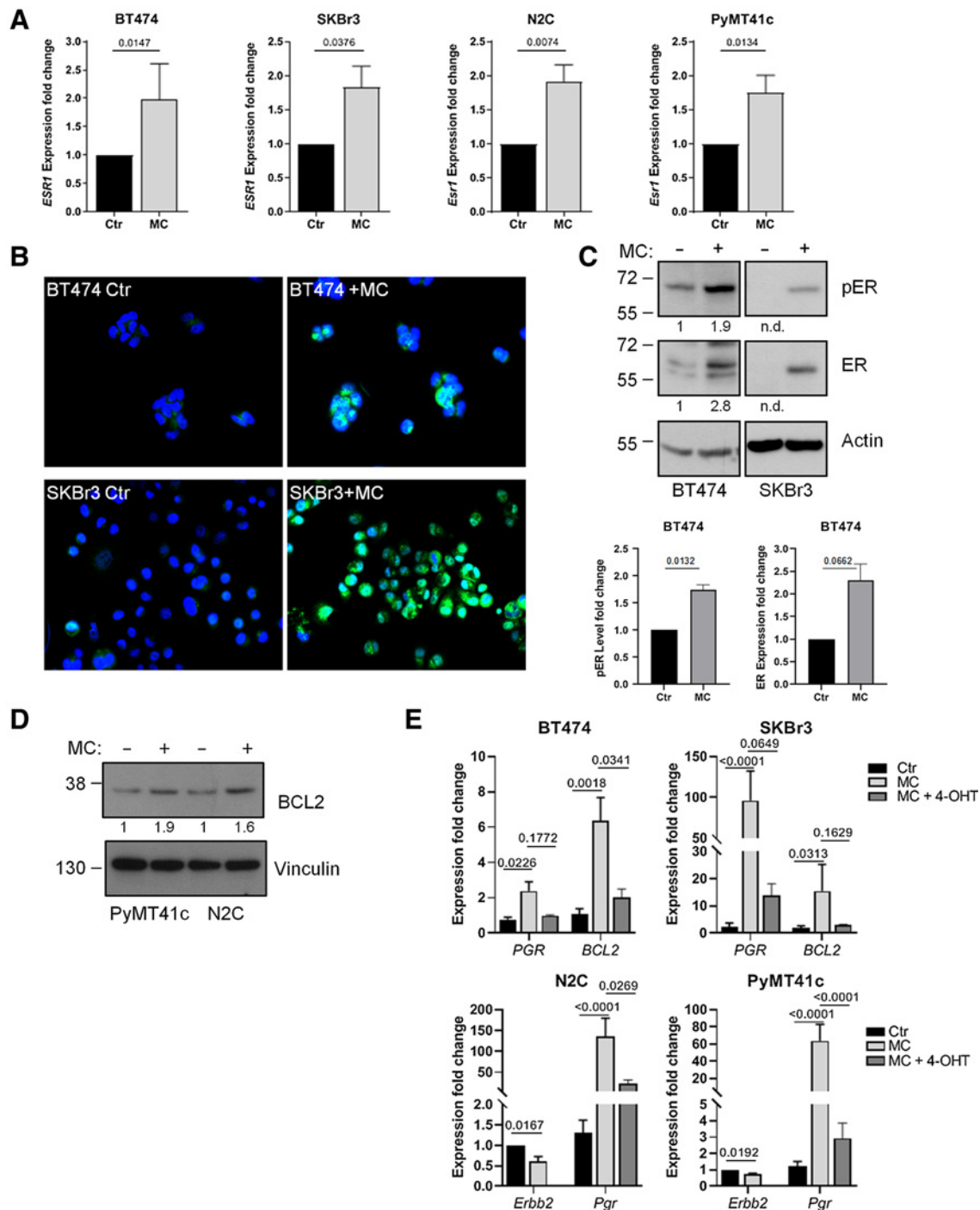
MCs negatively regulate the expression of the basal marker CK5. **A**, The abundance of infiltrating MCs is plotted according to breast cancer subtypes of the METABRIC dataset analyzed by CIBERSORT software. Only samples with a CIBERSORT $P < 0.05$ were included in the analysis. **B**, Box plots comparing the expression levels of the luminal *KRT8* and basal *KRT5* markers in the breast cancer subtypes of METABRIC dataset. **C**, Real-time PCR to evaluate the expression levels of the basal marker *Krt5* (CK5) in N2C murine cells ($n = 5$; two-tailed paired t test) and of the luminal marker *KRT8* (CK8) in human BT474 cells ($n = 3$; two-tailed paired t test), both cultured with (MC) or without (Ctr) BMMCs. **D**, Western blots showing the levels of CK5 in PyMT41c cells cocultured with BMMCs at increasing ratios. The coculture experiment was performed also with human SKBr3 and BT474 cell lines kept in coculture with BMMCs for 24 hours. **E**, MDA-MB-231 and BT474 cells were stimulated with TGF β (100 pmol/L for 24 hours) cocultured or not with BMMCs. Western blot analysis was performed to evaluate the levels of CK5 and CK8. **F**, The same experiment was performed by employing murine PyMT41c cells cocultured with MCs.

classification and it determines the choice of treatment. We therefore tested whether the coculture with MCs affects the expression of ER in a panel of breast cancer cell lines, both human- and mouse-derived. In all the cell lines tested, the presence of MCs caused a significant increase of ER transcription (Fig. 5A) and protein levels (Fig. 5B). Interestingly, this effect was observed also in the SKBr3 cell line, which is considered an ER-negative model, and, accordingly, it expresses barely detectable *ESR1* levels in real-time PCR (Supplementary Fig. S1D) and not detectable ER protein in untreated conditions (Fig. 5C). Because ER

appeared active according to its phosphorylation status (Fig. 5C), we investigated the expression of a number of genes known to be expressed in an ER-dependent manner and which can be assumed as surrogate markers of ER activation and luminal phenotype. As expected, *BCL2* (Fig. 5D and E) and *PGR* (Fig. 5E) levels were increased by MC coculturing, hence supporting the notion that MCs can increase both the levels and activity of ER. To further test whether the expression of these genes is indeed dependent on ER activity, we treated breast cancer cells cocultured with MCs with 4-OHT

**Figure 4.**

MCs reduce the basal phenotype through the inhibition of cMET receptor. **A**, Box plots showing cMET (left) and EGFR (right) expression in different breast cancer subtypes of the METABRIC dataset. **B**, Western blot analysis showing the levels of phosphorylated and total cMET in human triple-negative (MDA-MB-231 and BT549) and HER2-positive (SKBr3 and BT474) breast cancer cell lines after coculture with BMMCs (left) for 24 hours. Graphs show the effect of MC coculture on cMET phosphorylation in SKBr3 and BT474 cells (middle; $n = 4$; two-tailed paired t test). In addition, cMET-activated levels were evaluated in the same human cell lines cocultured with the human HMC1.2 mast cell line. **C**, EGFR activation was tested upon coculture with BMMCs. Graphs show the effect of MC coculture on EGFR phosphorylation in SKBr3 and BT474 cells ($n = 4$; two-tailed paired t test). **D**, BT474 cells were transfected with siRNAs specific for cMET and serum starved. After 72 hours from transfection, cells were stimulated with 20 ng/mL EGF for further 3 hours, in the presence or absence of BMMCs. Western blots show CK5 (top), cMET and CK8 (bottom) levels. Graphs show the levels of CK5 in BT474 cells silenced for cMET ($n = 3$; paired t test). **E**, The percentage of degranulated BMMCs was evaluated by measuring the percentage of CD107a⁺ MCs in untreated conditions upon stimulation with ionomycin for 30 minutes or after coculturing with the indicated breast cancer cell lines for 24 hours.

**Figure 5.**

The luminal phenotype is promoted by MCs through the increase of ER signaling. **A**, Real-time PCR showing the levels of ER (*ESR1*) gene expression in human (BT474, $n = 5$; SKBr3, $n = 5$; two-tailed paired t test) and murine (N2C, $n = 6$; PyMT41c, $n = 5$; two-tailed paired t test) cell lines cultured with or without BMMCs. **B**, Immunofluorescence performed on SKBr3 and BT474 cells with or without MCs to evaluate the levels of ER (green). **C**, Western blot analysis showing ER total and phosphorylation levels in BT474 and SKBr3 cells cocultured or not with MCs. Graphs show the effect of MC coculture on ER phosphorylation and ER total levels in BT474 cells ($n = 3$; two-tailed paired t test). ER level in SKBr3 cells cocultured with MCs was evaluated in four independent experiments and was not detectable in unstimulated conditions. n.d., signal not detectable. **D**, Expression of BCL2, a surrogate marker of ER activation, was detected through Western blotting in PyMT41c and N2C murine cell lines. **E**, MC-mediated stimulation of the ER activity is assessed by real-time PCR to evaluate *PGR* expression level in human ($n \geq 3$; two-tailed unpaired t test) and murine ($n \geq 4$; two-tailed unpaired t test) cell lines treated or not with 10 $\mu\text{mol/L}$ 4-OHT for 4 hours before harvesting. Expression of *BCL2* was assessed in human cell lines ($n \geq 3$; two-tailed unpaired t test). Expression levels of HER2 (*ErbB2*) were evaluated in mouse cells maintained with MCs compared with control cells ($n \geq 6$; two-tailed paired t test).

confirming that the upregulation of these expected ER targets was prevented. Interestingly, and in opposition to what observed with other genes, *ERBB2* expression levels were reduced by MC presence (Fig. 5E, bottom).

MCs activate a luminal signature in breast cancer cells

To test whether MCs are indeed able to promote a luminal phenotype, we performed gene expression profiling of 8 spontaneous mammary tumors from PyMT B6 and 7 from PyMT Wsh mice. We identified 61 genes differently expressed in a significant manner (FDR < 0.05), 38 up- and 23 down-regulated in PyMT B6 mice (Fig. 6A; Supplementary Table S1). As expected, PyMT B6 tumors expressed higher levels of MC-related genes (*Mcpt4*, *Cma1*, *Kit*) due to their infiltration within the tumors. GSEA showed that luminal breast cancer gene sets were positively enriched in a significant manner in PyMT B6 mice, while PyMT Wsh mice were characterized by a positive enrichment of basal gene sets (Fig. 6B). In addition, these luminal and basal gene sets were positively and negatively correlated, respectively, to the levels of infiltrating mast cells in METABRIC tumors (Fig. 6B). This analysis confirmed that B6 tumors are more characterized by a luminal phenotype while Wsh tumors showed an enrichment of basal and mesenchymal genes (Fig. 6B; Supplementary Fig. S2A). Although individually not significantly, a number of luminal and ER-related genes (*Scube2*, *Pgr*, and *Esr1* itself) were upregulated in B6 tumors, while *Krt5* was downregulated and ER levels were upregulated in B6 PyMT tumors also at protein level (Supplementary Fig. S2B).

Knowing that MCs are more infiltrated in luminal tumors (METABRIC database) and having shown that they promote a luminal phenotype and upregulate the expression of ER and its downstream targets, we investigated whether a correlation exists between MCs and the ER pathway also in breast cancer patients of the GHEA study, which enrolled patients with HER2-positive breast cancer treated with adjuvant trastuzumab. The MC-related gene *CPA3* positively correlated with *ESR1*, *PGR*, *BCL2*, and *SCUBE2* (Supplementary Fig. S3) while, in agreement with our evidence, *ERBB2* negatively correlated with MC presence (Supplementary Fig. S3). The reliability of *CPA3* as a marker of MC infiltration was confirmed by evaluating its correlation with *MS4A2*, which is another gene considered specific for MCs and correlates well with *CPA3* (Supplementary Fig. S3).

Having shown that MCs reduce the activation of pathways, which positively regulate the basal program and simultaneously promote the expression of several luminal markers, we tested the capacity of MCs to affect other signaling pathways by Proteome Profiler Mouse Phospho-RTK Array and found that they could reduce the activation of HER2 (Fig. 6C). This observation, together, with the reduced expression observed previously (Fig. 5E), prompted us to investigate the consequence of HER2 inhibition since HER2 activation is known to reduce ER expression (35). As expected, the silencing of HER2 was sufficient to induce the expression of ER and PGR, a surrogate marker of its activation (Fig. 6D). Moreover, also the inhibition of HER2 *in vivo*, by using the 7.16.4-sensitive N2C tumor, caused an increase of *Esr1* expression (Fig. 6E). This experiment also revealed a positive correlation between *Esr1* expression and MC density, further supporting the hypothesis that MCs could favor the development of a luminal phenotype (Fig. 6F).

MC density promotes the relapse of HER2-positive tumors upon treatment with anti-HER2 therapy

Because our findings support the notion that MCs could determine the phenotype of breast cancer cells, we asked whether they also affect the aggressiveness of HER2-positive tumors of patients with breast

cancer. To this end, we exploited gene expression data of 36 patients with HER2-positive breast cancer treated with adjuvant trastuzumab in the GHEA study. These patients were previously stratified in high or low risk of relapse according to the TRAstuzumab Risk (TRAR) signature, which includes 41 genes (31). Interestingly, we noticed that 6 of 14 genes upregulated in the TRAR-high group were MC-related (31) and confirmed that the levels of MCs, estimated *in silico* by CIBERSORT, were significantly higher in the TRAR-high group (Fig. 7A). Of note, *CPA3*, employed alone as a surrogate marker of MC abundance, was significantly more expressed in patients who indeed relapsed after treatment (Fig. 7B). Therefore, MC infiltration appears to be predictive of an increased risk of relapse in patients with HER2-positive breast cancer treated with adjuvant trastuzumab.

We then asked whether MCs could directly influence the response to therapy. Because of the lack of a HER2-positive model in a MC-deficient background, we employed N2C cells, which are sensitive to HER2-directed therapy and which were injected in the fat pad of syngeneic BALB/c mice together with or without BMMCs to mimic increased MC density. Mice were then treated with the anti-HER2 antibody 7.16.4. Although treatment significantly inhibited tumor growth in both groups, with or without adopted MCs (tumor volume inhibition 69.7% vs. 74.5%, respectively), at the end of the experiment, tumors were bigger in the group receiving MCs in coinjection (Fig. 7C and D). This observation prompted us to investigate whether the increased presence of MCs favored engraftment and, accordingly, we found that, after one week from the engraftment and before the starting of the treatment, tumors were significantly bigger (Fig. 7E). Therefore, although further experiments are required to assess whether MCs indeed protect cancer cells from anti-HER2 treatment and may eventually result in higher recurrence, our results strongly support the notion that MCs promote the tumor-initiating potential of breast cancer cells and stimulate the growth of established tumors.

Discussion

Our work provides evidence that MCs could play an active role in breast cancer outcome by affecting directly the phenotype of cancer cells. We show here that, in PyMT mice, the presence of MCs favors the development of larger tumors, which arise earlier, and are hence characterized by higher grade and enhanced metastasis to lungs, compared with MCs-void PyMT Wsh mice. On the other hand, in the absence of MCs, tumors display basal and squamous features more frequently. In accordance to these *in vivo* findings, our *in vitro* experiments show that MCs prevent the activation of the master regulator of the basal program cMET (36) and simultaneously stimulate the expression and activity of the luminal-associated ER (37).

Our results are clinically relevant, as ER is a crucial receptor in patients with breast cancer and it is exploited to classify tumor subtypes (38) and, consequently, select the therapeutic strategy (3). Notably, ER profoundly affects also the intrinsic biological features of cancer cells (39). It regulates the expression of genes that play a role in a plethora of cellular activities such as cell proliferation, migration, and survival (40). Luminal breast cancer tumors, consistently with our findings, are more infiltrated by MCs and are characterized by ER (and/or PGR) expression (41, 42). Luminal breast cancers are usually associated with better prognosis (43). However, ER activation stimulates prosurvival pathways also (44) and hence it is not surprising that ER expression is linked to increased risk of relapse in patients with breast cancer treated in adjuvant settings with trastuzumab (31) and that it negatively impacts on the efficacy of anti-HER2-based

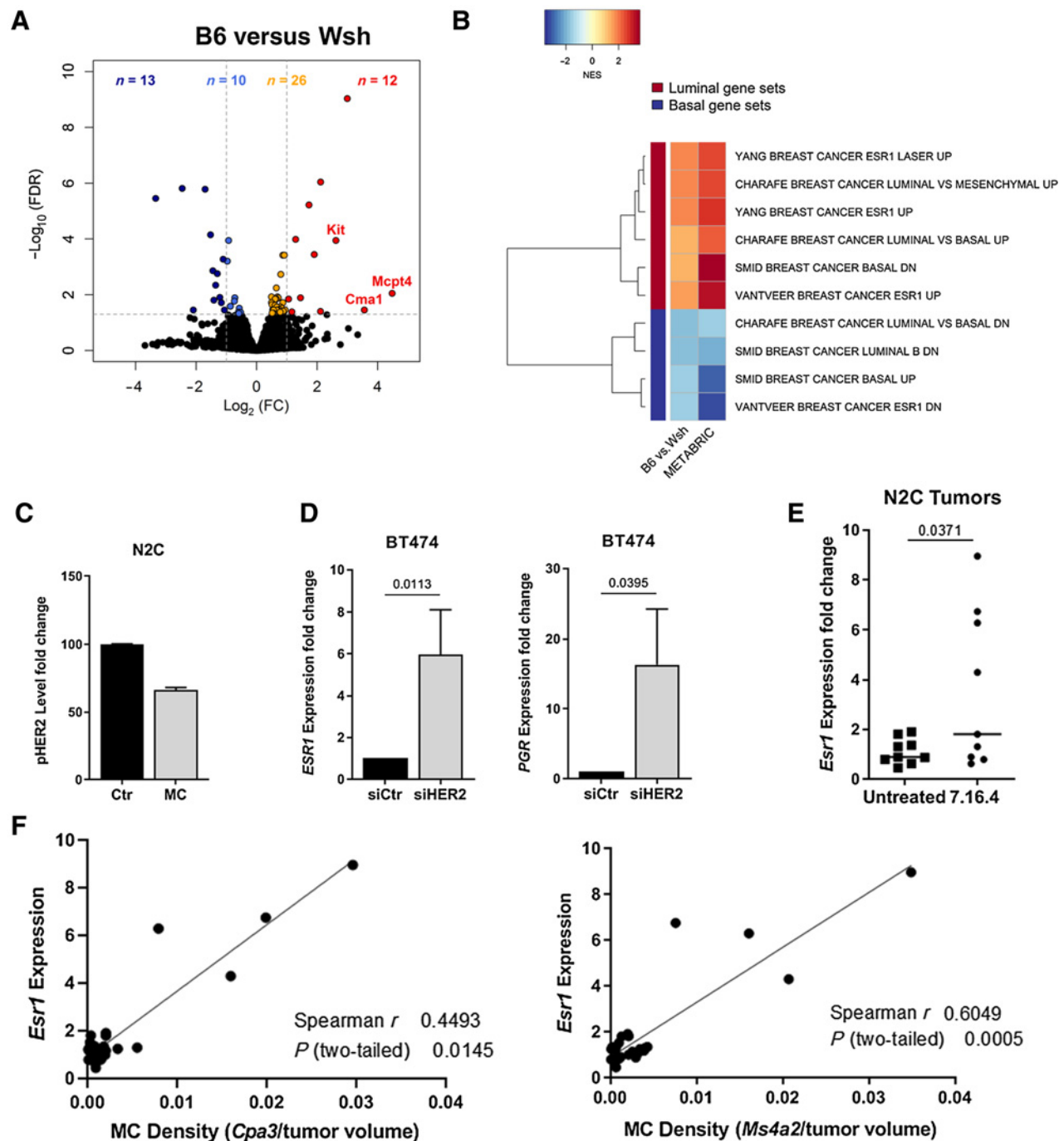


Figure 6.

MCs stimulate ER activity with consequent activation of a luminal program. **A**, Volcano plot showing differentially expressed genes between PyMT B6 and PyMT Wsh mice. On the x-axis the \log_2 of the fold change is shown, while the y-axis reports the $-\log_{10}$ of the FDR. The horizontal dashed line represents an FDR of 0.05; vertical dashed lines represent a fold change of 2 and -2 . Darker colors highlight significant genes with a fold change ≥ 2 . **B**, The heatmap shows the normalized enrichment score (NES) of the luminal and basal breast cancer gene sets that are significantly enriched (FDR < 0.05) in the comparison between B6 and Wsh mice and that are significantly correlated to MC infiltration in METABRIC dataset. **C**, N2C cells were cocultured with MCs for 24 hours and then analyzed by mouse phospho-RTK Array. Relative levels of phosphorylated HER2 in the absence (Ctr) or presence (MC) of MCs are shown. **D**, Expression levels of *ESR1* (left; $n = 3$; two-tailed paired t test) and *PGR* (right; $n = 3$; two-tailed paired t test) evaluated in BT474 cells silenced for HER2 and compared with control cells transfected with a nontargeting siRNA. **E**, Expression of *Esr1* in N2C tumors collected from BALB/c mice treated with 7.16.4 or left untreated (9 mice/group; two-tailed unpaired t test). **F**, Correlation between *Esr1* expression and *Cpa3* (left) or *Ms4a2* (right) expression, the MC genes normalized on tumor volume, in N2C tumors collected from BALB/c mice treated with 7.16.4 injections or left untreated as shown in **E**.

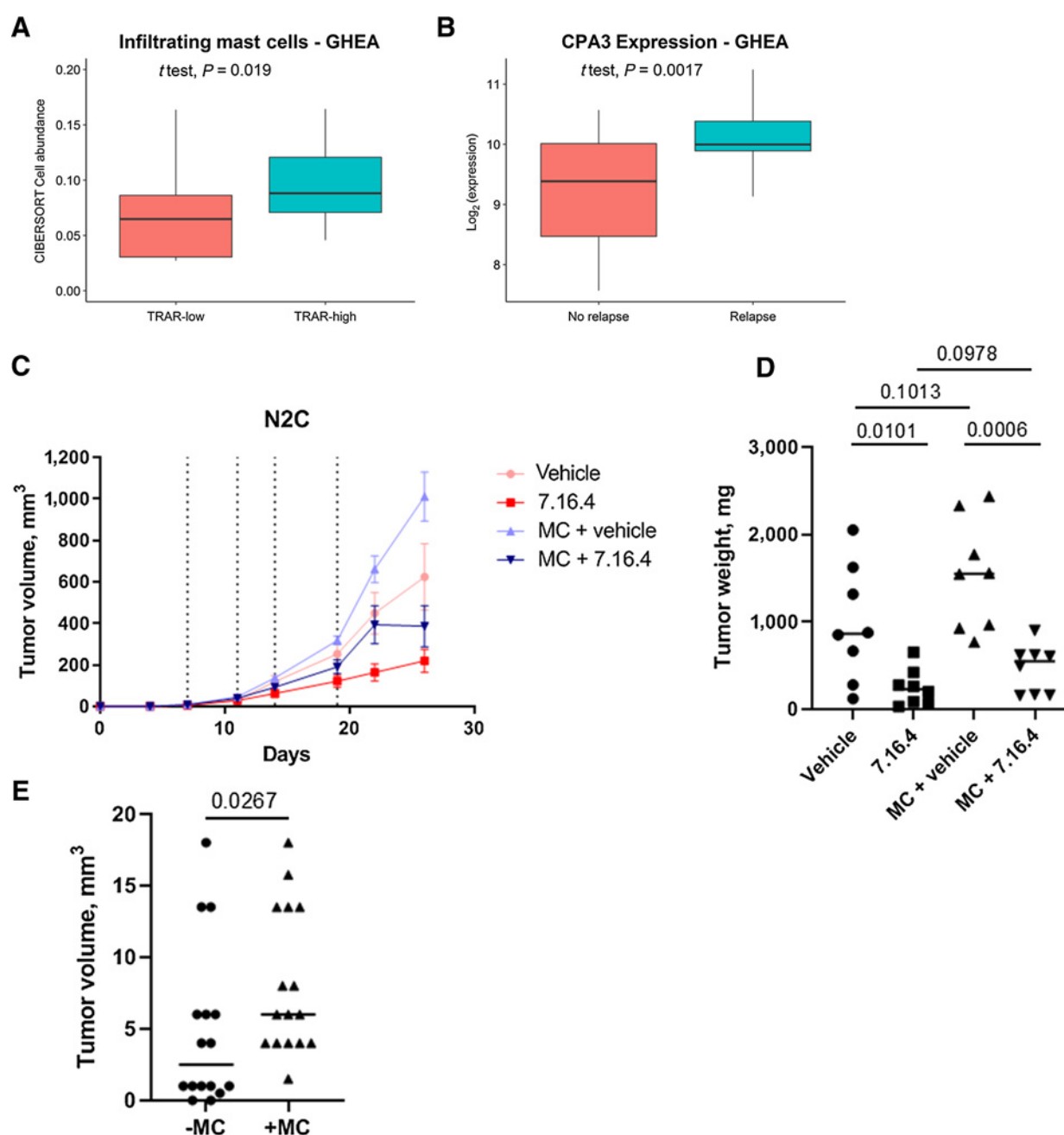


Figure 7.

MCs infiltrating the tumor increase the risk of relapse upon trastuzumab treatment. **A**, Evaluation of the tumor-infiltrating MC abundance, estimated by CIBERSORT, in patients of the GHEA dataset divided in TRAR-high and TRAR-low risk of relapse upon adjuvant treatment with trastuzumab. **B**, The same analysis was performed by using only *CPA3* expression to evaluate the level of MC infiltration in patients stratified on the basis of the occurrence of relapse or not. **C**, BALB/c mice were engrafted with N2C alone or coinjected with BMMCs and treated or not with 7.16.4. Tumor volumes are shown. **D**, Graph showing the tumor weights evaluated at the end of the experiment (8 animals/group; two-tailed unpaired *t* test). **E**, Tumor volumes of N2C tumors measured at day 7, before treatment started. Statistical significance was calculated by two-tailed Mann-Whitney test.

therapy (45). Recently, the capacity of MCs to hinder the effectiveness of treatment has been reported also in patients with inflammatory breast cancer treated with neoadjuvant chemotherapy (23). In that work, close proximity of MCs with CD8 T cells and CD163 monocytes/macrophages was associated with reduced response to therapy supporting the idea that MCs could contribute to an immunosuppressive

microenvironment in patients with breast cancer (23). The latter notion was supported also by evidence derived from TRAMP prostate cancer *in vivo* models, which proved a cross-talk between MCs and MDSCs (21). Importantly, in those settings, the presence/absence of MCs influenced the rate of adenocarcinoma versus neuroendocrine tumors arising in TRAMP mice (21, 28), hence suggesting that MCs

can contribute to cancer cell plasticity. Our work further supports this notion by demonstrating that MCs, together with the modulation of the immune tumor microenvironment, can also perturb directly adjacent cancer cells (20). Notably, MC absence mainly affected the phenotype of the external region of mammary nodules, which constitutes the area where the vast majority of MCs localizes in our PyMT B6 model.

Our findings showing that MCs presence promotes tumor growth and metastasis are in agreement with previous evidence (46), even though the underlying mechanisms have so far not been investigated. Here, we provide evidence that MCs can stimulate the ER pathway and this could contribute to cancer cell outgrowth. Of note, it has been shown that MCs can also affect normal mammary gland development and that the absence of these immune cells results in defective branching and delayed duct formation (47). This effect was attributed to the capacity of MCs to shape the stromal microenvironment of mammary glands, but our work supports the fascinating scenario that MCs could support mammary gland development also by favoring ER expression and activity, which is crucial during mammary development.

In our settings, MCs appear to promote tumor growth both in spontaneous PyMT and in transplantable models, but do not affect significantly the efficacy of the treatment at least in terms of tumor volume inhibition. This does not exclude that, at a single-cell level, a few cancer cells adjacent to MCs could acquire resistance to treatment and be responsible for the formation of relapse following the treatment. Further work will be necessary to clarify the latter point. In fact, the main limitation of the presented work is that we could not perform *in vivo* experiments with HER2-positive breast cancer models and compare completely MC-deprived mice versus mice reconstituted with MCs due to technical reasons. In fact, BALB/c mice are MC-proficient and hence MCs infiltrate N2C tumors even when not coinjected with cancer cells. Nevertheless, tumors engraftment appeared earlier and tumors were larger in the presence of adoptive MCs, suggesting that increased number of MCs correlates with enhanced tumor growth. On the other hand, we tried to reconstitute PyMT Wsh mice with intraperitoneal and intravenous injections of BMDCs, which did not reconstitute the mammary tissue differently to what observed, for example, in prostate tumors (21). On the contrary, adoptive transferred MCs localized in the spleen and, in very few cases, in lungs (our observations) and BMDCs injected directly into the glands would require a long time to fully engraft (47), not compatible with the development of spontaneous PyMT tumors. However, both spontaneous and transplantable models, along with our *in vitro* coculture experiments confirmed that MCs indeed promote a luminal phenotype, characterized by increased ER levels and expression of ER target genes.

In conclusion, our work supports the notion that MCs could play a role in breast cancer outcome also by affecting the phenotype of cancer

cells. Their role could be dual: protect from basal tumors, which are known to be extremely aggressive, and promote the expression of a luminal phenotype through the activation of the ER pathway. Although the latter effect is generally considered a good prognostic factor, in HER2-positive breast cancer it is associated with treatment failure and could eventually promote relapse. Because MCs are relatively few within the tumor microenvironment compared with other immune population, they could affect the features of a restricted number of cancer cells and determine the onset of small areas, which could be, for example, resistant to therapy. This would allow the production of single cancer cells with the potential to generate relapse and/or metastasis, without evidently affecting the pathologic response. Further work is still necessary to dissect the intrinsic mechanisms by which MCs stimulate the activity of ER and to determine whether they could be exploited as markers of clinical outcome or even as actionable targets. However, our work demonstrates for the first time that MCs are important players in tumor aggressiveness by modulating the phenotype of cancer cells.

Disclosure of Potential Conflicts of Interest

No potential conflicts of interest were disclosed.

Authors' Contributions

Conception and design: C. Tripodo, M.P. Colombo, D. Lecis

Development of methodology: M.T. Majorini, L. De Cecco, E. Fontanella, D. Lecis

Acquisition of data (provided animals, acquired and managed patients, provided facilities, etc.): V. Cancila, A. Rigoni, L. Botti, T. Triulzi, L. De Cecco, E. Jachetti, C. Chiodoni, C. Tripodo

Analysis and interpretation of data (e.g., statistical analysis, biostatistics, computational analysis): M.T. Majorini, V. Cancila, M. Dugo, L. De Cecco, E. Jachetti, E. Tagliabue, C. Chiodoni, C. Tripodo, D. Lecis

Writing, review, and/or revision of the manuscript: M.T. Majorini, T. Triulzi, E. Tagliabue, M.P. Colombo, D. Lecis

Administrative, technical, or material support (i.e., reporting or organizing data, constructing databases): T. Triulzi, E. Fontanella

Study supervision: M.P. Colombo, D. Lecis

Acknowledgments

This work was supported by 5 × 1000 Funds–2013, Italian Ministry of Health (to D. Lecis) and Associazione Italiana per la Ricerca sul Cancro (Investigator Grant number 18425 to M.P. Colombo). Maria Teresa Majorini was supported by a Fondazione Umberto Veronesi fellowship. We are grateful to Chiara Maura Ciniselli and Paolo Verderio (INT) for advice on statistical analysis, Giovanna Talarico (INT) for the support with FACS analysis, Barbara Cappetti and Renata Ferri (INT) for technical assistance.

The costs of publication of this article were defrayed in part by the payment of page charges. This article must therefore be hereby marked *advertisement* in accordance with 18 U.S.C. Section 1734 solely to indicate this fact.

Received November 14, 2019; revised February 4, 2020; accepted March 11, 2020; published first March 16, 2020.

References

1. Siegel RL, Miller KD, Jemal A. Cancer statistics, 2019. *CA Cancer J Clin* 2019;69:7–34.
2. Bastien RR, Rodriguez-Lescure A, Ebbert MT, Prat A, Munarriz B, Rowe L, et al. PAM50 breast cancer subtyping by RT-qPCR and concordance with standard clinical molecular markers. *BMC Med Genomics* 2012;5:44.
3. Prat A, Pineda E, Adamo B, Galvan P, Fernandez A, Gaba L, et al. Clinical implications of the intrinsic molecular subtypes of breast cancer. *Breast* 2015;24:S26–35.
4. Coates AS, Winer EP, Goldhirsch A, Gelber RD, Gnant M, Piccart-Gebhart M, et al. Tailoring therapies—improving the management of early breast cancer: St Gallen international expert consensus on the primary therapy of early breast cancer 2015. *Ann Oncol* 2015;26:1533–46.
5. Gil Del Alcazar CR, Huh SJ, Ekram MB, Trinh A, Liu LL, Beca F, et al. Immune escape in breast cancer during in situ to invasive carcinoma transition. *Cancer Discov* 2017;7:1098–115.
6. Pages F, Galon J, Dieu-Nosjean MC, Tartour E, Sautes-Fridman C, Fridman WH. Immune infiltration in human tumors: a prognostic factor that should not be ignored. *Oncogene* 2010;29:1093–102.
7. Issa-Nummer Y, Darb-Esfahani S, Loibl S, Kunz G, Nekljudova V, Schrader I, et al. Prospective validation of immunological infiltrate for prediction of

- response to neoadjuvant chemotherapy in HER2-negative breast cancer—a substudy of the neoadjuvant GeparQuinto trial. *PLoS One* 2013;8:e79775.
8. Gentles AJ, Newman AM, Liu CL, Bratman SV, Feng W, Kim D, et al. The prognostic landscape of genes and infiltrating immune cells across human cancers. *Nat Med* 2015;21:938–45.
 9. Denkert C, Loibl S, Noske A, Roller M, Muller BM, Komor M, et al. Tumor-associated lymphocytes as an independent predictor of response to neoadjuvant chemotherapy in breast cancer. *J Clin Oncol* 2010;28:105–13.
 10. Adams S, Gray RJ, Demaria S, Goldstein L, Perez EA, Shulman LN, et al. Prognostic value of tumor-infiltrating lymphocytes in triple-negative breast cancers from two phase III randomized adjuvant breast cancer trials: ECOG 2197 and ECOG 1199. *J Clin Oncol* 2014;32:2959–66.
 11. De Mattos-Arruda L, Sammut SJ, Ross EM, Bashford-Rogers R, Greenstein E, Markus H, et al. The genomic and immune landscapes of lethal metastatic breast cancer. *Cell Rep* 2019;27:2690–708.
 12. Gabrilovich DI. Myeloid-derived suppressor cells. *Cancer Immunol Res* 2017;5:3–8.
 13. Sica A, Larghi P, Mancino A, Rubino L, Porta C, Totaro MG, et al. Macrophage polarization in tumour progression. *Semin Cancer Biol* 2008;18:349–55.
 14. Valeta-Magara A, Gadi A, Volta V, Walters B, Arju R, Ghashuddin S, et al. Inflammatory breast cancer promotes development of M2 tumor-associated macrophages and cancer mesenchymal cells through a complex chemokine network. *Cancer Res* 2019;79:3360–71.
 15. De Angelis C, Nagi C, Hoyt CC, Liu L, Roman K, Wang C, et al. Evaluation of the predictive role of tumor immune infiltrate in HER2-positive breast cancer patients treated with neoadjuvant anti-HER2 therapy without chemotherapy. *Clin Cancer Res* 2020;26:738–745.
 16. Hamy AS, Bonsang-Kitzis H, De Croze D, Laas E, Darrigues L, Topciu L, et al. Interaction between molecular subtypes and stromal immune infiltration before and after treatment in breast cancer patients treated with neoadjuvant chemotherapy. *Clin Cancer Res* 2019;25:6731–41.
 17. Bense RD, Sotiriou C, Piccart-Gebhart MJ, Haanen JB, van Vugt MA, de Vries EG, et al. Relevance of tumor-infiltrating immune cell composition and functionality for disease outcome in breast cancer. *J Natl Cancer Inst* 2016;109:djw192. DOI: 10.1093/jnci/djw192.
 18. Rigoni A, Bongiovanni L, Burocchi A, Sangaletti S, Danelli L, Guarnotta C, et al. Mast cells infiltrating inflamed or transformed gut alternatively sustain mucosal healing or tumor growth. *Cancer Res* 2015;75:3760–70.
 19. Rigoni A, Colombo MP, Pucillo C. Mast cells, basophils and eosinophils: from allergy to cancer. *Semin Immunol* 2018;35:29–34.
 20. Rigoni A, Colombo MP, Pucillo C. The role of mast cells in molding the tumor microenvironment. *Cancer Microenviron* 2015;8:167–76.
 21. Jachetti E, Cancila V, Rigoni A, Bongiovanni L, Cappetti B, Belmonte B, et al. Cross-talk between myeloid-derived suppressor cells and mast cells mediates tumor-specific immunosuppression in prostate cancer. *Cancer Immunol Res* 2018;6:552–65.
 22. Piconese S, Gri G, Tripodo C, Musio S, Gorzanelli A, Frossi B, et al. Mast cells counteract regulatory T-cell suppression through interleukin-6 and OX40/OX40L axis toward Th17-cell differentiation. *Blood* 2009;114:2639–48.
 23. Reddy SM, Reuben A, Barua S, Jiang H, Zhang S, Wang L, et al. Poor response to neoadjuvant chemotherapy correlates with mast cell infiltration in inflammatory breast cancer. *Cancer Immunol Res* 2019;7:1025–35.
 24. Sangaletti S, Stoppacciaro A, Guiducci C, Torrisi MR, Colombo MP. Leukocyte, rather than tumor-produced SPARC, determines stroma and collagen type IV deposition in mammary carcinoma. *J Exp Med* 2003;198:1475–85.
 25. Conti A, Majorini MT, Fontanella E, Bardelli A, Giacca M, Delia D, et al. Lemur tyrosine kinase 2 (LMTK2) is a determinant of cell sensitivity to apoptosis by regulating the levels of the BCL2 family members. *Cancer Lett* 2017;389:59–69.
 26. Guy CT, Cardiff RD, Muller WJ. Induction of mammary tumors by expression of polyomavirus middle T oncogene: a transgenic mouse model for metastatic disease. *Mol Cell Biol* 1992;12:954–61.
 27. Nagle DL, Kozak CA, Mano H, Chapman VM, Bucan M. Physical mapping of the *tec* and *Gabrb1* loci reveals that the *wsh* mutation on mouse chromosome 5 is associated with an inversion. *Hum Mol Genet* 1995;4:2073–9.
 28. Pittoni P, Tripodo C, Piconese S, Mauri G, Parenza M, Rigoni A, et al. Mast cell targeting hampers prostate adenocarcinoma development but promotes the occurrence of highly malignant neuroendocrine cancers. *Cancer Res* 2011;71:5987–97.
 29. Ritchie ME, Phipson B, Wu D, Hu Y, Law CW, Shi W, et al. Limma powers differential expression analyses for RNA-sequencing and microarray studies. *Nucleic Acids Res* 2015;43:e47.
 30. Curtis C, Shah SP, Chin SF, Turashvili G, Rueda OM, Dunning MJ, et al. The genomic and transcriptomic architecture of 2,000 breast tumours reveals novel subgroups. *Nature* 2012;486:346–52.
 31. Triulzi T, De Cecco L, Sandri M, Prat A, Giussani M, Paolini B, et al. Whole-transcriptome analysis links trastuzumab sensitivity of breast tumors to both HER2 dependence and immune cell infiltration. *Oncotarget* 2015;6:28173–82.
 32. Newman AM, Liu CL, Green MR, Gentles AJ, Feng W, Xu Y, et al. Robust enumeration of cell subsets from tissue expression profiles. *Nat Methods* 2015;12:453–7.
 33. Subramanian A, Tamayo P, Mootha VK, Mukherjee S, Ebert BL, Gillette MA, et al. Gene set enrichment analysis: a knowledge-based approach for interpreting genome-wide expression profiles. *Proc Natl Acad Sci U S A* 2005;102:15545–50.
 34. Raymond WW, Cruz AC, Caughey GH. Mast cell and neutrophil peptidases attack an inactivation segment in hepatocyte growth factor to generate NK4-like antagonists. *J Biol Chem* 2006;281:1489–94.
 35. Guo S, Sonenshein GE. Forkhead box transcription factor FOXO3a regulates estrogen receptor alpha expression and is repressed by the her-2/neu/phosphatidylinositol 3-kinase/akt signaling pathway. *Mol Cell Biol* 2004;24:8681–90.
 36. Gastaldi S, Sassi F, Accornero P, Torti D, Galimi F, Migliardi G, et al. Met signaling regulates growth, repopulating potential and basal cell-fate commitment of mammary luminal progenitors: implications for basal-like breast cancer. *Oncogene* 2013;32:1428–40.
 37. Di-Cicco A, Petit V, Chiche A, Bresson L, Romagnoli M, Orian-Rousseau V, et al. Paracrine met signaling triggers epithelial-mesenchymal transition in mammary luminal progenitors, affecting their fate. *Elife* 2015;4:e06104. DOI: 10.7554/eLife.06104.
 38. Vasconcelos I, Hussainzada A, Berger S, Fietze E, Linke J, Siedentopf F, et al. The St. Gallen surrogate classification for breast cancer subtypes successfully predicts tumor presenting features, nodal involvement, recurrence patterns and disease free survival. *Breast* 2016;29:181–5.
 39. Bouris P, Skandalis SS, Piperigkou Z, Afratis N, Karamanou K, Aletras AJ, et al. Estrogen receptor alpha mediates epithelial to mesenchymal transition, expression of specific matrix effectors and functional properties of breast cancer cells. *Matrix Biol* 2015;43:42–60.
 40. Bourdeau V, Deschenes J, Metivier R, Nagai Y, Nguyen D, Bretschneider N, et al. Genome-wide identification of high-affinity estrogen response elements in human and mouse. *Mol Endocrinol* 2004;18:1411–27.
 41. Carpeno E, Ceausu RA, Cimpean AM, Gaje PN, Saptefrati L, Fulga V, et al. Mast cells as an indicator and prognostic marker in molecular subtypes of breast cancer. *In Vivo* 2019;33:743–8.
 42. Glajcar A, Szpor J, Pacek A, Tyrak KE, Chan F, Streb J, et al. The relationship between breast cancer molecular subtypes and mast cell populations in tumor microenvironment. *Virchows Arch* 2017;470:505–15.
 43. Prat A, Perou CM. Deconstructing the molecular portraits of breast cancer. *Mol Oncol* 2011;5:5–23.
 44. Sun M, Paciga JE, Feldman RI, Yuan Z, Coppola D, Lu YY, et al. Phosphatidylinositol-3-OH kinase (PI3K)/AKT2, activated in breast cancer, regulates and is induced by estrogen receptor α (ER α) via interaction between ER α and PI3K. *Cancer Res* 2001;61:5985–91.
 45. Loi S, Dafni U, Karlis D, Polydoropoulou V, Young BM, Willis S, et al. Effects of estrogen receptor and human epidermal growth factor receptor-2 levels on the efficacy of trastuzumab: a secondary analysis of the HERA trial. *JAMA Oncol* 2016;2:1040–7.
 46. He L, Zhu Z, Chen S, Wang Y, Gu H. Mammary tumor growth and metastasis are reduced in c-kit mutant sash mice. *Cancer Med* 2016;5:1292–7.
 47. Lilla JN, Werb Z. Mast cells contribute to the stromal microenvironment in mammary gland branching morphogenesis. *Dev Biol* 2010;337:124–33.